Nanoscale

PAPER

View Article Online
View Journal | View Issue

CrossMark click for updates

Cite this: *Nanoscale*, 2015, **7**, 17812

Spin Seebeck effect and spin Hall magnetoresistance at high temperatures for a Pt/yttrium iron garnet hybrid structure

Shuanhu Wang,[a] Lvkuan Zou,[a] Xu Zhang,[a] Jianwang Cai,[a] Shufang Wang,*[b] Baogen Shen[a] and Jirong Sun*[a]

Received 13th August 2015, Accepted 21st September 2015

DOI: 10.1039/c5nr05484b

www.rsc.org/nanoscale

Based on unique experimental setups, the temperature dependences of the longitudinal spin Seebeck effect (LSSE) and spin Hall magnetoresistance (SMR) of the Pt/yttrium iron garnet (Pt/YIG) hybrid structure are determined in a wide temperature range up to the Curie temperature of YIG. From a theoretical analysis of the experimental relationship between the SMR and temperature, the spin mixing conductance of the Pt/YIG interface is deduced as a function of temperature. Adopting the deduced spin mixing conductance, the temperature dependence of the LSSE is well reproduced based on the magnon spin current theory. Our research sheds new light on the controversy about the theoretical models for the LSSE.

1. Introduction

Due to the strong spin–orbit coupling of Pt and the distinct ferromagnetic properties of yttrium iron garnet (YIG), the spin and charge transport of the Pt/YIG hybrid structure exhibits novel phenomena. An intriguing discovery is the spin Seebeck effect in Pt/YIG,[1–5] stemming from thermal gradient-caused spin current injection from YIG into Pt. This effect provides a new approach for the generation and manipulation of spin current, and thus has drawn great attention in recent years. In addition to the spin Seebeck effect, the spin Hall magnetoresistance (SMR) of Pt/YIG is also an interesting discovery.[6] It has been proven that the charge current in Pt produces a vertical spin current due to the spin Hall effect, and the reflection of this spin current at the Pt/YIG interface then generates a charge current that is superimposed on the original one, leading to a new kind of magnetoresistance.

Although the physical image of the SMR is very clear, the mechanism for the spin Seebeck effect, particularly the longitudinal spin Seebeck effect (LSSE), is still in debate. Two representative theories have been presented by Xiao *et al.* and Rezende *et al.*, respectively. Xiao *et al.*[7–11] believed that the magnon, electron and phonon temperatures are different at the Pt/YIG interface, though the expected temperature differences are not observed from the analysis of the Brillouin light scattering spectra,[12] and this generates spin pumping into Pt, yielding the LSSE. Different from Xiao *et al.*, Rezende *et al.*[13] ascribed the LSSE to the temperature gradient-generated magnon spin current across YIG, and presented a theory that well reproduced the temperature dependence of the LSSE obtained below room temperature. Both theories describe incoherent spin pumping, but, in the latter theory, magnon propagation & accumulation induced by heat current is taken into consideration. By studying the temporal evolution of the LSSE, Agrawal *et al.*[14] found that the thermal gradient rose faster than the LSSE signal, which means that bulk magnon transport plays an important role in determining the LSSE. Despite the controversy of the different theoretical models, there is a consensus that the spin mixing conductance (G), spin Hall angle (θ_{sh}) and spin diffusion length (λ_{Pt}) are important factors affecting both the LSSE and the SMR. This implies that these two effects may mutually corroborate, leading to further insights into the underlying physics.

We noted that most of the previous experiments on the LSSE and SMR have been performed in the low temperature region, *i.e.*, below room temperature. Data for the high temperature region, particularly near the Curie temperature (T_C) of YIG, are scarce because of experimental difficulties, though they are particularly important for elucidating the mechanisms of the LSSE and SMR. Recently, Uchida *et al.*[15] undertook the only study on high temperature LSSE, and observed a rapid decrease of the LSSE voltage (V_{LSSE}) with an increase in temperature, *i.e.*, $V_{LSSE} \propto (T_C - T)^3$. It is a pity that the reported V_{LSSE} fluctuates around zero in the temperature range of 450 to 520 K. This and the lack of a simultaneous study on the SMR make a comprehensive analysis of the LSSE and SMR difficult. Based on unique experimental setups, in this paper we determined the LSSE and the SMR for the same Pt/YIG hybrid struc-

[a]*Beijing National Laboratory for Condensed Matter Physics and Institute of Physics, Chinese Academy of Sciences, Beijing 100190, People's Republic of China. E-mail: jrsun@iphy.ac.cn*
[b]*College of Physics Science and Technology, Hebei University, Baoding 071002, Hebei Province, People's Republic of China. E-mail: swang2008@hotmail.com*

ture in a wide temperature range below T_C. From the SMR data, the temperature-dependent spin mixing conductance was determined. A rapid decrease of G with an increase of temperature is observed above 300 K, due to the reduction of the magnetization of YIG. Adopting the parameters deduced from the SMR, the temperature dependence of the LSSE is satisfactorily reproduced with the theory of magnon spin current. These analyses show that the spin mixing conductance of the Pt/YIG interface, the magnetization of YIG and the spin diffusion length of Pt strongly influence the LSSE.

2. Experiment

A 21 μm-thick single crystal YIG slab was first grown above (111)-oriented $Gd_3Ga_5O_{12}$ (5 × 3 × 0.5 mm^3) by liquid phase epitaxy, and then a Pt layer with a thickness of 7 nm or 30 nm was deposited, *via* magnetron sputtering, on the top of YIG through a Hall-bar-shaped mask. To generate a vertical thermal gradient (∇T), the sample was heated by an underneath ceramic heater that is pasted to the sample by silver epoxy. In this case, the temperature gradient is directed from bottom to top. An alternative method to generate the thermal gradient is illuminating the top of the sample using a laser beam while heating the sample back with the heater.[14,16–18] In this case, the thermal gradient is directed from top to bottom for the present laser power (30 mW). The magnetic field (H) is provided by a Helmholtz coil, applied along the x-axis of the sample. Two electrodes aligning along the y-axis are used to detect the LSSE voltage. The whole measurement unit, including the sample, the heater, the laser emitter and the Helmholtz coil, is sealed in an electromagnetic shielding box in an ambient atmosphere. The SMR is measured using the physical property measurement system (PPMS) in the temperature range below 300 K and a home-made system above 300 K. The magnetic field is applied in the x–y plane at an angle of 45° with respect to the x-axis. The laser has a power of 30 mW and a wavelength of 660 nm. The spot size of the laser is ~4.6 mm in diameter, nearly covering the whole Pt Hall bar.

3. Results and discussion

Fig. 1b and c show the magnetic field dependences of the thermal voltage, recorded in the temperature range from 300 K to 516 K in the thermal gradient generated by heater alone

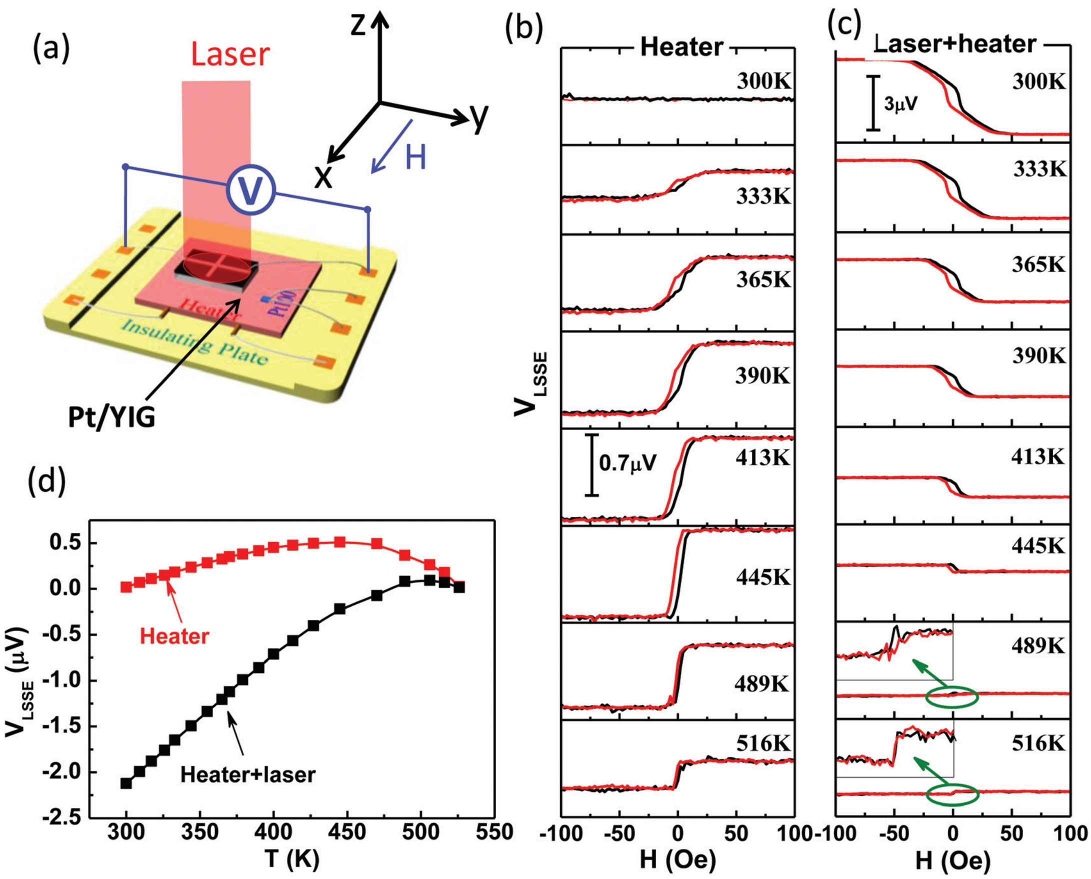

Fig. 1 (a) A schematic showing the experimental setup for the LSSE study. A ceramic heater is placed underneath Pt/YIG and a laser beam is focused on the sample surface. The average temperature of the sample is measured by a Pt100 thermometer on the heater. (b) and (c) Magnetic field dependences of the thermal voltage across the Pt bar, generated by the thermal gradient of heater (b) and heater plus laser (c), respectively. (d) LSSE voltage as a function of temperature.

(1b) and the heater plus laser (1c), respectively. Around ambient temperature, as shown in Fig. 1b, the sample is at thermal equilibrium with the environment and no thermoelectric voltage changes are observed for magnetic cycling. The V_{LSSE} appears when the sample is heated above 300 K, grows with heating power and, after a maximum value of 1 μV at ~445 K, decreases rapidly. This complex behavior could be jointly determined by the variation of the thermal gradient, magnetization and thermal conductivity of YIG.[7] Under the combined influence of the heater and laser beam, an opposite V_{LSSE}–H loop is detected up to 489 K, implying a reversion of the thermal gradient direction. Possibly, the laser heating generates a local thermal gradient that over-counteracts that of the heater. In this case, the V_{LSSE} is maximal at room temperature, and continuously decreases with the increase of temperature. Fig. 1d is a summary of the LSSE voltage, deduced from the difference of the two thermoelectric voltages under, respectively, a positive and a negative saturation field. It clearly shows the systematic variation of V_{LSSE} with temperature.

Obviously, the complex temperature dependence of V_{LSSE} in Fig. 1d is determined by the variations of the thermal gradient, magnetization of YIG, spin mixing conductance of Pt/YIG, and spin diffusion length of Pt, *etc*. To get a quantitative description of the LSSE, it is necessary to determine the thermal gradient as a function of temperature. In general, a direct measurement of the temperature difference for the top and bottom planes of YIG will cause considerable experimental errors. As an alternative, we adopted a two-dimensional finite element model (2D FEM) to simulate the temperature distribution in YIG. During the simulation, the bottom plane of YIG was set to a temperature between 300 K and 560 K, and the environment to 300 K. Heat exchange was assumed to occur on the top surface, *via* thermal radiation. The parameters involved in this simulation such as heat conductivity and heat capacity are obtained from ref. 19 and 20. Please refer to Appendix A for details of the FEM calculation. As an example, the thermal distributions for an average sample temperature of 415 K are shown in Fig. 2c and d, respectively corresponding to the cases with and without laser illumination. Since the Pt strip for the thermoelectric measurements is located exactly in the middle of the top plane of YIG, we choose the temperature distribution just underneath the Pt strip to evaluate the thermal gradient (dashed line in Fig. 2c and d). Since the temperature changes linearly from the top to the bottom of YIG, the thermal gradient is a constant. Fig. 2e shows the deduced ∇T as a function of sample temperature. As expected, the thermal gradient generated by the heater exhibits monotonic growth with sample temperature, varying from 0 to 540 K

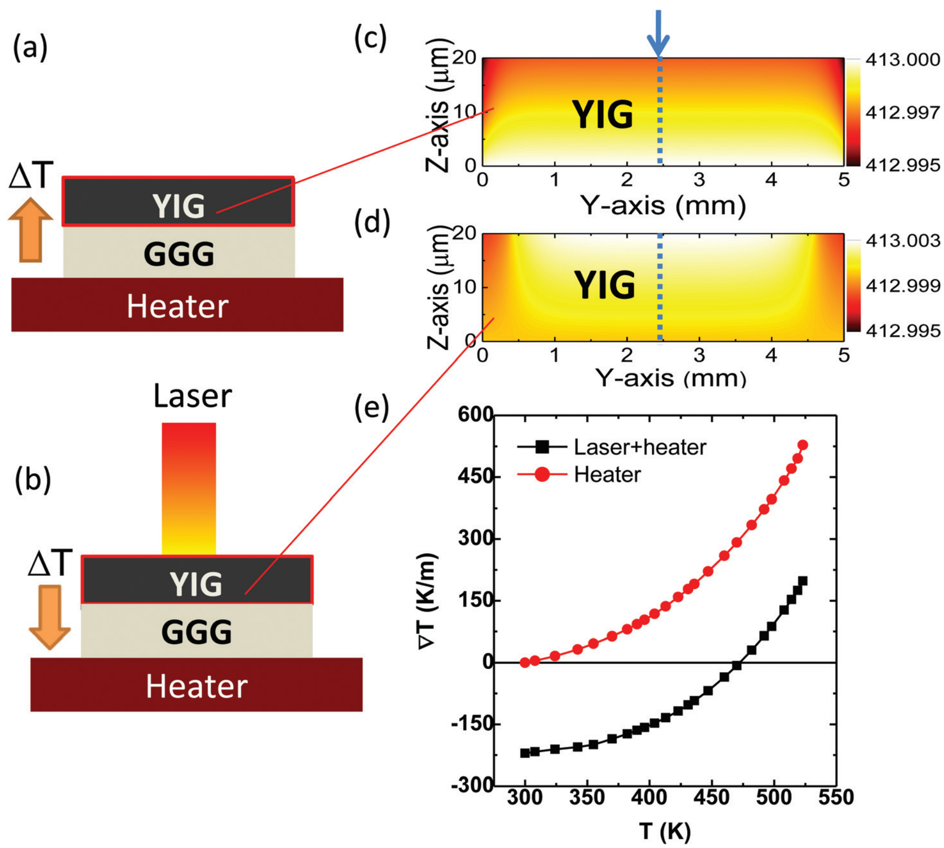

Fig. 2 Experiment setups for the generation of thermal gradient by heater (a) and heater plus laser (b). (c) and (d) Temperature distribution in YIG on the cross section just below the Pt strip for thermoelectric measurements. The average sample temperature is 413 K. (e) Temperature gradient as a function of sample temperature, obtained along the middle of the YIG (marked by dashed lines).

m^{-1} as the temperature increases from 300 K to 530 K. In contrast, the ∇T produced by the combined heater and laser shows a direction reversion at ~475 K. Below ~475 K, the effect of local heating by the laser is dominant, and ∇T points to the $-z$ direction. However, with the increase of temperature, the effect of the heater finally counteracts that of the laser, and the direction of ∇T is reversed. We noted that, at room temperature, the ∇T generated here by the laser is similar to that obtained by Agrawal *et al.*[14] using a laser of 70 mW.

Based on the results of the 2D FEM calculations, we get the temperature dependence of $V_{LSSE}/\nabla T$ in Fig. 3a. The $V_{LSSE}/\nabla T$ data for the two different heating methods coincide with each other satisfactorily. The meaning of this result is two-fold. First, the temperature gradient thus obtained is reasonable. Second, the experiment data are reliable. As shown in Fig. 3a, $V_{LSSE}/\nabla T$ is ~10 nVm K^{-1} at 300 K, it decreases monotonically with the increase of temperature, and vanishes as T approaches T_C. We also performed the experiments for a sample with a thicker Pt strip (30 nm), and observed a similar temperature dependence (inset in Fig. 3a). These results reveal a weakening of the LSSE as the temperature approaches T_C, qualitatively agreeing with those of Uchida *et al.*[15]

On plotting $V_{LSSE}/\nabla T$ against T_C-T in double logarithmic scale, we obtained a good linear relationship that shows a slope of ~1.5. This means a critical exponent lower than that reported by Uchida *et al.*[15] The YIG film employed here is much thinner than that used by Uchida *et al.* (21 μm *vs.* 1 mm). This could be the reason for this difference, noting the variation of the temperature dependence of the LSSE with the YIG thickness.[21] A similar analysis was performed on the data of the 30 nm Pt, and the same temperature dependence of V_{LSSE} was observed, which reveals the generality of these phenomena.

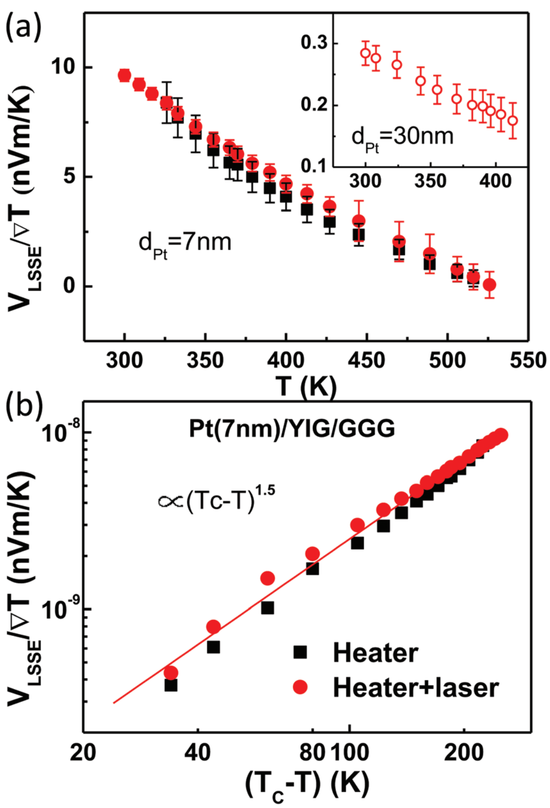

Fig. 3 (a) Temperature dependence of $V_{LSSE}/\nabla T$ for two different heating methods. Inset shows the data of the sample with a thicker Pt strip (30 nm). (b) Double logarithmic plot of the T_C-T dependence of $V_{LSSE}/\nabla T$. Solid line is a guide for the eye.

Obviously, the magnetization of YIG, the spin Hall angle of Pt and the spin mixing conductance of the Pt/YIG interface may vary significantly with temperature, especially as T approaches T_C. All of these will affect the LSSE, resulting in a dramatic variation of the V_{LSSE} with T. To understand the specific temperature dependence, a thorough analysis of the $V_{SSE}-T$ relationship is desired. As aforestated, there is a consensus that the spin mixing conductance, spin Hall angle, spin diffusion length are important factors determining both the LSSE and the SMR. Considering the fact that different effects may mutually corroborate with each other, an investigation on the temperature dependence of the SMR may be helpful for a thorough understanding of the $V_{SSE}-T$ dependence. Fig. 4a is schematic showing the experimental setup. A relatively large measuring current of 500 μA was applied along the Pt layer in order to offset the unbalanced LSSE voltage background generated by thermal irradiation. This current will not generate significant Joule heating as demonstrated by previous research.[22] The voltage signals were collected from two transversally aligned electrodes, as a function of the magnetic field which is applied at an angle of 45° with respect to the x-axis (also the easy magnetization axis of YIG) and cycled between −100 Oe and 100 Oe. Here transversal resistivity ρ_{xy} is acquired to characterize the SMR because of its low background signal and thus high signal-to-noise ratio. Fig. 4b shows ρ_{xy} as a function of the applied field, measured at different temperatures. ρ_{xy} is nearly constant above the saturation field, increases rapidly as H decreases and reaches a maximum at $H = 0$. These are typical features of the SMR. With the decrease of temperature, the resistivity change $\Delta\rho_{xy}$ exhibits first, rapid growth when the temperature is high, and then a slow decrease when the temperature is low, leaving a local maximum of 5.6×10^{-4} at ~97.6 K (Fig. 4c).

In general, from the temperature dependence of the SMR, additional information can be obtained such as the spin mixing conductance, spin Hall angle, and spin diffusion length. As reported, the SMR can be well described by

$$\frac{\Delta\rho_{xy}}{\rho} = \theta_{sh}^2 \frac{\lambda_{Pt}}{t_{Pt}} \frac{2\lambda_{Pt} G \tanh^2 \frac{t_{Pt}}{2\lambda_{Pt}}}{\sigma_{Pt} + 2\lambda_{Pt} G \coth \frac{t_{Pt}}{\lambda_{Pt}}}, \tag{1}$$

where θ_{sh}, λ_{Pt}, t_{Pt} and σ_{Pt} are the spin Hall angle, spin diffusion length, thickness and conductivity of Pt, respectively. The equality $\Delta\rho_{xy} = \Delta\rho_{xx}$ has been adopted here.[6,23]

Through careful analysis, Marmion *et al.*[24] found that temperature dependence of the SMR is mainly affected by λ_{Pt} below room temperature,[25] determined by the Elliot–Yafet mechanism for spin relaxation. Alternatively, Meyer *et al.*[26] ascribed

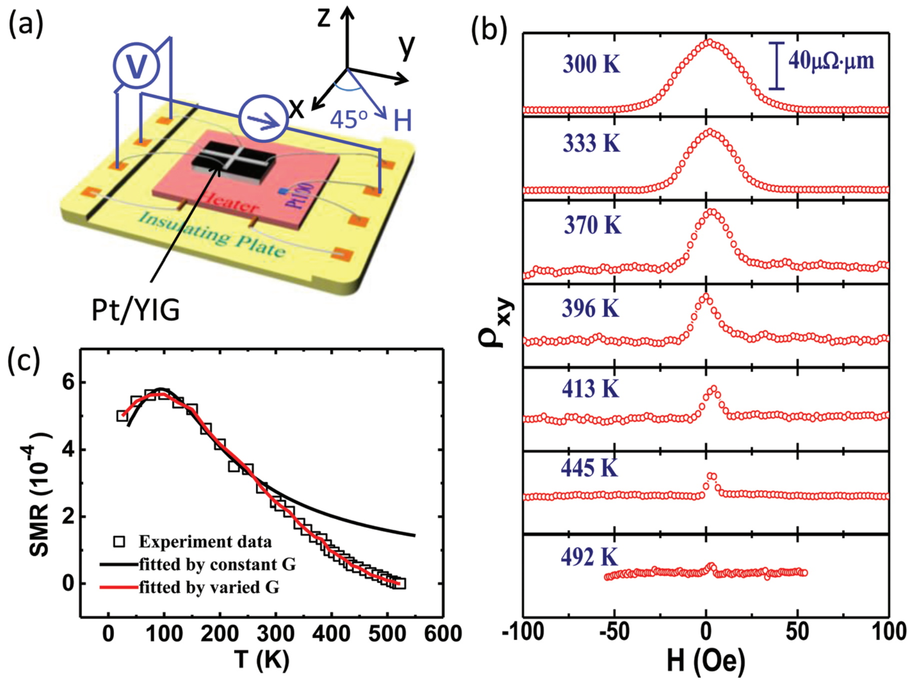

Fig. 4 Experimental setup for the measurement of SMR. A heater is used to heat the sample. (b) Magnetic field dependence of the transversal resistivity ρ_{xy} above 300 K. (c) Comparison of the experimental SMR (open symbols) with theoretical results (solid lines). The black and red curves are calculated by eqn (1) adopting a constant and a varied spin mixing conductance (G), respectively.

the variation of the SMR to a decrease in θ_{sh} instead of λ_{Pt}. According to Meyer *et al.*, θ_{sh} changes obviously below 100 K whereas it remains nearly constant above 100 K. In contrast, Isasa *et al.*[27] declared that θ_{sh} was relatively weakly temperature-dependent, and the λ_{Pt} decay with an increase in temperature, in the form of the Elliot–Yafet mechanism, is the origin of the temperature effects. Obstbaum *et al.*[28] studied the inverse spin Hall effect and anisotropic magnetoresistance for the Pt/permalloy structure, and found that a good agreement of the experimental results with theoretical ones is gained only when θ_{sh} is a constant. As for G, both Marmion[24] and Meyer[26] treated it as a constant below 300 K, independent of temperature.

Based on the above work, we firstly fit our experimental data to eqn (1), adopting a constant θ_{sh} (0.085), and G (9×10^{14} Ω^{-1} m^{-2}), and varied λ_{Pt} of the Elliot–Yafet form ($\lambda_{Pt} = 3 \times 10^{-7}/T$ in unit of nm). As shown by Fig. 4c, although the experimental data (symbols) can be satisfactorily reproduced at low temperatures (black curve), obvious deviations appear above 280 K. Considering the obvious change of the magnetic properties of YIG with temperature, high temperature may mainly influence the spin mixing conductance. Therefore, setting G to a constant could be inadequate at high temperatures. By setting G to

$$G = \frac{\sigma_{Pt}}{\left(\dfrac{2\lambda_{Pt}\theta_{sh}^2 G\lambda_{Pt}\tanh^2\left(\dfrac{t_{Pt}}{2\lambda_{Pt}}\right)}{\dfrac{\Delta\rho_{xy}}{\rho}t_{Pt}} - 2\lambda_{Pt}\coth\left(\dfrac{t_{Pt}}{\lambda_{Pt}}\right)\right)}, \quad (2)$$

we obtained the temperature dependence G shown in Fig. 5. G is nearly constant below 280 K and decreases linearly with an increase of temperature above 280 K, where θ_{sh} has been set to 0.085, and σ_{Pt} has been obtained by direct measurements. Indeed, reduced magnetization of YIG causes a reduction in G. We noted that a similar G–T relationship has been theoretical predicted by Ohnuma *et al.*[29] and experimentally deduced by Uchida *et al.*[30] The red curve in Fig. 4c demonstrates the self-consistent fitting of the SMR data.

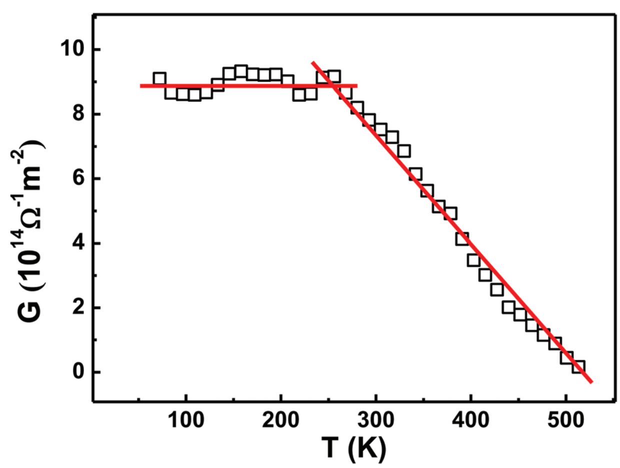

Fig. 5 Temperature dependence of spin mixing conductance G deduced from SMR based on eqn (2).

Adopting the deduced G–T relationship, the temperature dependence of $V_{\rm LSSE}$ can be calculated based on different theoretical models. Xiao *et al.* proposed a model based on the spin pumping generated by the difference of magnon and electron (phonon) temperatures [eqn (11) in Appendix B].[7–10] Later, Rezende *et al.*[9] presented an alternative model based on the bulk magnon spin current in YIG, generated by the thermal gradient (eqn (15) in Appendix B). In the latter model, the temperature dependence of the magnon lifetime is considered, and a rigid magnon dispersion relationship is adopted. Eqn (15) has well explained the temperature dependence of the LSSE below room temperature. Details of these two theories are presented in Appendix B. The parameters involved in eqn (11) and (15) can be directly measured, such as the resistivity of Pt, or indexed from references (refer to Appendix B for details).

In Fig. 6 we show a comparison of the experimental (symbols) and theoretical (solid curves) results. The olive and blue curves are calculated by the theories of Xiao *et al.* and Rezende *et al.*, respectively. Different from the experimental result, the theoretical $V_{\rm LSSE}/\nabla T$ of Xiao *et al.* displays a progressive increase with temperature to a local maximum at ~470 K, before a drastic drop at higher temperatures. It is not clear at present whether the oversimplified magnon dispersion relationship of this theory is responsible for this strong deviation. In contrast, the magnon spin current theory proposed by Rezende *et al.* yields results that are in good agreement with the experimental ones. The slight deviations in the temperature interval from 400 K to 500 K could be ascribed to inaccurate parameters adopted for the calculations (for example, the magnon diffusion length $l_{\rm m}$ may be temperature dependent rather than independent[31]). It implies that the LSSE can be produced without referring to the difference of magnon and phonon temperatures at the Pt/YIG interface. According to this theory, the LSSE is associated with the magnon spin current across YIG, and it is thus a bulk effect. Recently, Etesami *et al.*[32] presented a model by solving the stochastic Landau–Lifshitz–Gilbert equation, and they found that the LSSE can be an effect of magnon accumulation, quantified by exchange spin torque, which also support the scenario of the bulk origin of the LSSE.

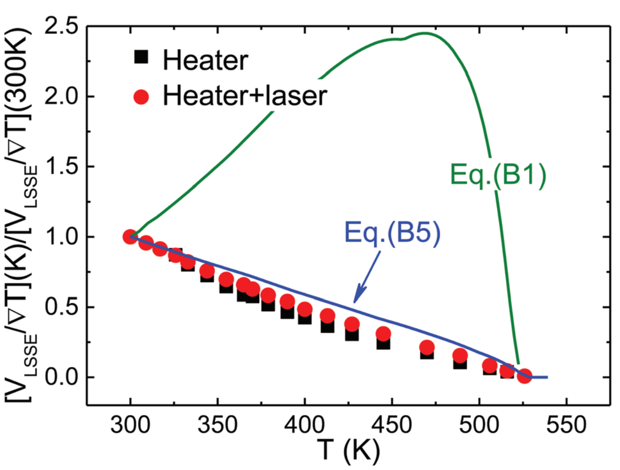

Fig. 6 Comparison of experimental (symbols) and theoretical (solid curves) results. Olive and blue curves are obtained from the theories proposed by Xiao *et al.* and Rezende *et al.*, respectively.

4. Summary

The temperature dependence of the LSSE and SMR has been experimentally studied for the Pt/YIG hybrid structure. Based on two different experimental setups, two sets of LSSE voltages that coincide with each other have been obtained as functions of sample temperature, adopting the thermal gradients determined by finite element calculations. Simultaneously, SMR was recorded as a function of temperature. Through the analysis of SMR, spin mixing conductance is derived. The decrease of the magnetization of YIG results in a linear reduction of the spin mixing conductance with an increase in temperature when the latter is higher than 300 K. Adopting the deduced spin mixing conductance and the independently adjusted spin diffusion length and spin Hall angle, the temperature dependence of the LSSE is well reproduced based on the magnon spin current theory. The present work provides a deep insight to the mechanism of the LSSE and other spin transport processes in the Pt/YIG hybrid structure.

Appendix A: detail in 2D FEM

For the temperature gradient induced by thermal radiation,

$$k\nabla T = \varepsilon\sigma({T_{\rm amb}}^4 - T^4) \quad (3)$$

where k is the thermal conductivity of YIG and $T_{\rm amb}$ is the ambient temperature which is 300 K. For YIG, $\varepsilon_{\rm YIG}$ = 0.5.[33] k is calculated by $k = DC_{\rm p}\rho$, where D, $C_{\rm p}$ and ρ are thermal diffusivity, heat capacity and density. For YIG, ρ = 5170 kg m^{-3},[34] and the temperature dependences of D and $c_{\rm p}$ are extracted from ref. 19 and 20, respectively.

The reflectivity at the interface between layer $i-1$ and layer i is calculated by the Fresnel equation[9]

$$R = \left|\frac{n_{i-1} - n_i}{n_{i-1} + n_i}\right|^2, \quad (4)$$

where n_i denotes the refractive index[35–37] and we get $R_{\rm Pt/air}$ = 0.17, $R_{\rm YIG/Pt}$ = 0.009, $R_{\rm YIG/air}$ = 0.15. There are two kinds of surface exposed to the illumination. One is covered by Pt and the other is not, as shown in Fig. 7.

For the surface covered by Pt, the reflected energy as shown in Fig. 7 is $Q_{\rm r1}^{\rm Pt} \approx 0$ and $Q_{\rm r2}^{\rm Pt} \approx 0$. The energy of the laser is $Q_{\rm in0}$ = 2.5 mW mm^{-2}. The input energy at the interface between Pt and YIG (noted as 1) after being reflected and absorbed by Pt is

$$Q_{\rm in1}^{\rm Pt}(z_{\rm pt} = 7\ {\rm nm}) = Q_{\rm in0}(1 - R_{\rm Pt/air})e^{-\alpha_{\rm Pt}z_{\rm Pt}} = 0.468Q_{\rm in0}. \quad (5)$$

Energy passed through the YIG film is

$$Q_{\rm in2}^{\rm Pt}(z_{\rm YIG} = 20\ \mu{\rm m}) = Q_{\rm in1}^{\rm Pt}(1 - R_{\rm YIG/Pt})e^{-\alpha_{\rm YIG}z_{\rm YIG}} = 0.172Q_{\rm in0}. \quad (6)$$

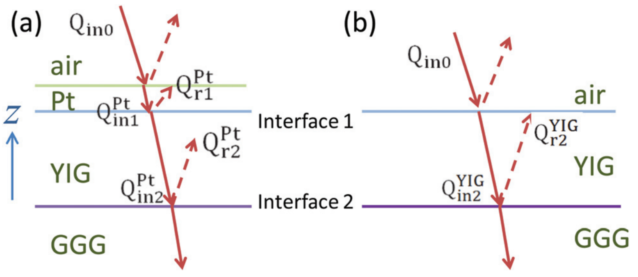

Fig. 7 Sample surface coved by Pt (a) and YIG (b).

So the energy absorbed by YIG in this case is

$$Q_{abs}^{Pt} = Q_{in1}^{Pt} - Q_{in2}^{Pt} - Q_{r2} = 0.296Q_{in0}. \tag{7}$$

For the surface covered by YIG, the energy passed through the YIG film is

$$Q_{in2}^{YIG}(z_{YIG} = 20\ \mu m) = Q_{in0}(1 - R_{YIG/air})e^{-\alpha_{YIG}z_{YIG}} = 0.313Q_{in0}. \tag{8}$$

Here energy absorbed by YIG is

$$Q_{abs}^{YIG} = Q_{in0} - Q_{in2}^{YIG} - Q_{r2}^{YIG} = 0.537Q_{in0}. \tag{9}$$

Due to the fact that the ratio of the surface covered by Pt and YIG is 15 : 85, the total energy absorbed by YIG is

$$Q_{abs} = 0.15Q_{abs}^{Pt} + 0.85Q_{abs}^{YIG} = 1.25\ \text{mW mm}^{-2}. \tag{10}$$

So during the FEM calculation, we applied a heat flow with a density of 1.25 mW mm^{-2} to the YIG film.

Appendix B: two kinds of theories for LSSE

Based on the interfacial thermal spin pumping mechanism[7,8,10] and the quadratic dispersion relationship, Xiao *et al.*[7,8] and Weiler *et al.*[10] found the inverse spin Hall effect voltage detected by Pt with the equation

$$V_{LSSE} = \frac{g\gamma\hbar k_B}{2\pi M_s V_a}\theta_{sh}\rho_{Pt}l_{Pt}\Delta T, \tag{11}$$

where the V_a is magnetic coherence volume and it is given by

$$V_a = \frac{2}{3\zeta(5/2)}\left(\frac{4\pi S}{k_B T}\right)^{3/2}. \tag{12}$$

$\hbar$ and k_B are the reduced Planck and Boltzmann constants. g is the spin mixing conductance per unit of interface area and the conductance quantum: $g = Gh/e^2$. M_s, γ and S are the saturation magnetization, gyromagnetic ratio and spin wave stiffness of YIG, respectively. It is reported that the spin wave stiffness is proportional to magnetization,[38,39] so

$$\frac{S(T)}{M(T)} = \frac{S(0)}{M(0)}. \tag{13}$$

At room temperature, $S(300\ \text{K}) = 8.5 \times 10^{-40}$ J m^2 (ref. 39). θ_{sh} is the spin-Hall angle of Pt which is shown to exhibit weak temperature dependence especially above 100 K.[27,28]

The mechanism proposed by Rezende *et al.*[13] for the LSSE is based on the magnon spin current generated in the bulk of the Pt, which provides continuity for the spin flow. The magnon dispersion relationship is

$$\omega_k = \omega_{ZB}\left(1 - \cos\frac{\pi k}{2k_m}\right), \tag{14}$$

where ω_{ZB} is the zone boundary frequency and k_m is the value of the maximum wave number.[13] They also considered magnon lifetime as a strong function of the wave number and found the spin current injected into Pt is

$$J_S^z = -\frac{\gamma\hbar\rho k_m^3 l_m}{4\pi M\pi^2}\frac{B_1 B_s}{B_2}gk_B\nabla T, \tag{15}$$

where ρ is the effect of the finite FMI layer thickness, noted as

$$\rho = \frac{\cosh(t_{FM}/l_m) - 1}{\sinh(t_{FM}/l_m)}. \tag{16}$$

k_m is the value of the maximum wave number:

$$k_m = \sqrt{3} \times 2.5/a_l = 2 \times 10^{-7}\text{cm}^{-1},$$

a_l being the lattice parameter, and magnon diffusion length l_m = 70 nm. The integrals B_1, B_2 and B_3 are noted as

$$B_1 = \int_0^1 q^2\frac{xe^x}{(e^x - 1)^2}dq, \tag{17a}$$

$$B_2 = \int_0^1 q^2\sin^2\left(\frac{\pi q}{2}\right)\frac{e^x}{\eta_q(e^x - 1)^2}dq \tag{17b}$$

and

$$B_s = \int_0^1 q^2\sin^2\left(\frac{\pi q}{2}\right)\frac{e^x x}{\eta_q(e^x - 1)^2}dq, \tag{17c}$$

where $x = \hbar\omega_k/(k_B/T)$, $q = k_m/k$, and $\eta_q = 1 + 500q(T/300) + (5100q^2 - 3250q^3)(T/300)^2$. By integrating the charge-current density along the Pt layer, the inverse spin Hall effect voltage detected in Pt becomes[40]

$$V_{LSSE} = R_{Pt}\omega\lambda_{Pt}\frac{2e}{\hbar}\theta_{SH}\tanh\left(\frac{t_{Pt}}{2\lambda_{Pt}}\right)J_S^z \tag{18}$$

where R_{Pt}, ω and t_{Pt} are resistance, thickness and width of the Pt strip, respectively.

Acknowledgements

The authors thank Erjia Guo (Institut für Physik, Johannes Gutenberg-Universität Mainz) for valuable discussions. This work has been supported by the National Basic Research of China (Grant No. 2011CB921801, 2012CB921403, and 2013CB921700), the National Natural Science Foundation of China (Grant No. 11074285, 51372064, and 11134007), and the Strategic Priority Research Program of the Chinese Academy of Sciences (XDB07030200).

References

1 K. Uchida, H. Adachi, T. Ota, H. Nakayama, S. Maekawa and E. Saitoh, *Appl. Phys. Lett.*, 2010, **97**, 172505–172503.
2 T. Kikkawa, K. Uchida, Y. Shiomi, Z. Qiu, D. Hou, D. Tian, H. Nakayama, X. F. Jin and E. Saitoh, *Phys. Rev. Lett.*, 2013, **110**, 067207.
3 J. H. Han, C. Song, F. Li, Y. Y. Wang, G. Y. Wang, Q. H. Yang and F. Pan, *Phys. Rev. B: Condens. Matter*, 2014, **90**, 144431.
4 T. Liao, J. Lin, G. Su, B. Lin and J. Chen, *Nanoscale*, 2015, **7**, 7920–7926.
5 D. Matatagui, O. V. Kolokoltsev, N. Qureshi, E. V. Mejia-Uriarte and J. M. Saniger, *Nanoscale*, 2015, **7**, 9607–9613.
6 H. Nakayama, M. Althammer, Y. T. Chen, K. Uchida, Y. Kajiwara, D. Kikuchi, T. Ohtani, S. Geprags, M. Opel, S. Takahashi, R. Gross, G. E. Bauer, S. T. Goennenwein and E. Saitoh, *Phys. Rev. Lett.*, 2013, **110**, 206601.
7 J. Xiao, G. E. W. Bauer, K.-c. Uchida, E. Saitoh and S. Maekawa, *Phys. Rev. B: Condens. Matter*, 2010, **81**, 214418.
8 J. Xiao, G. E. W. Bauer, K.-c. Uchida, E. Saitoh and S. Maekawa, *Phys. Rev. B: Condens. Matter*, 2010, **82**, 099904.
9 M. Schreier, A. Kamra, M. Weiler, J. Xiao, G. E. W. Bauer, R. Gross and S. T. B. Goennenwein, *Phys. Rev. B: Condens. Matter*, 2013, **88**, 094410.
10 M. Weiler, M. Althammer, M. Schreier, J. Lotze, M. Pernpeintner, S. Meyer, H. Huebl, R. Gross, A. Kamra, J. Xiao, Y. T. Chen, H. Jiao, G. E. Bauer and S. T. Goennenwein, *Phys. Rev. Lett.*, 2013, **111**, 176601.
11 J. C. Rojas-Sanchez, N. Reyren, P. Laczkowski, W. Savero, J. P. Attane, C. Deranlot, M. Jamet, J. M. George, L. Vila and H. Jaffres, *Phys. Rev. Lett.*, 2014, **112**, 106602.
12 M. Agrawal, V. I. Vasyuchka, A. A. Serga, A. D. Karenowska, G. A. Melkov and B. Hillebrands, *Phys. Rev. Lett.*, 2013, **111**, 107204.
13 S. M. Rezende, R. L. Rodriguez-Suarez, R. O. Cunha, A. R. Rodrigues, F. L. A. Machado, G. A. F. Guerra, J. C. L. Ortiz and A. Azevedo, *Phys. Rev. B: Condens. Matter*, 2014, **89**, 014416.
14 M. Agrawal, V. I. Vasyuchka, A. A. Serga, A. Kirihara, P. Pirro, T. Langner, M. B. Jungfleisch, A. V. Chumak, E. T. Papaioannou and B. Hillebrands, *Phys. Rev. B: Condens. Matter*, 2014, **89**, 224414.
15 K. Uchida, T. Kikkawa, A. Miura, J. Shiomi and E. Saitoh, *Phys. Rev. X*, 2014, **4**, 041023.
16 M. Walter, J. Walowski, V. Zbarsky, M. Munzenberg, M. Schafers, D. Ebke, G. Reiss, A. Thomas, P. Peretzki, M. Seibt, J. S. Moodera, M. Czerner, M. Bachmann and C. Heiliger, *Nat. Mater.*, 2011, **10**, 742–746.
17 M. Weiler, M. Althammer, F. D. Czeschka, H. Huebl, M. S. Wagner, M. Opel, I. M. Imort, G. Reiss, A. Thomas, R. Gross and S. T. Goennenwein, *Phys. Rev. Lett.*, 2012, **108**, 106602.
18 W. Lin, M. Hehn, L. Chaput, B. Negulescu, S. Andrieu, F. Montaigne and S. Mangin, *Nat. Commun.*, 2012, **3**, 744.
19 M. Guillot, F. Tchéou, A. Marchand, P. Feldmann and R. Lagnier, *Z. Phys. B: Condens. Matter*, 1981, **44**, 53–57.
20 A. M. Hofmeister, *Phys. Chem. Miner.*, 2006, **33**, 45–62.
21 T. Kikkawa, K. Uchida, S. Daimon, Z. Y. Qiu, Y. Shiomi and E. Saitoh, *Phys. Rev. B: Condens. Matter*, 2015, **92**, 064413.
22 W. X. Wang, S. H. Wang, L. K. Zou, J. W. Cai, Z. G. Sun and J. R. Sun, *Appl. Phys. Lett.*, 2014, **105**, 182403.
23 Y.-T. Chen, S. Takahashi, H. Nakayama, M. Althammer, S. Goennenwein, E. Saitoh and G. Bauer, *Phys. Rev. B: Condens. Matter*, 2013, **87**, 144411.
24 S. R. Marmion, M. Ali, M. McLaren, D. A. Williams and B. J. Hickey, *Phys. Rev. B: Condens. Matter*, 2014, **89**, 220404.
25 R. J. Elliott, *Phys. Rev.*, 1954, **96**, 266–279.
26 S. Meyer, M. Althammer, S. Geprags, M. Opel, R. Gross and S. T. B. Goennenwein, *Appl. Phys. Lett.*, 2014, **104**, 242411.
27 M. Isasa, E. Villamor, L. E. Hueso, M. Gradhand and F. Casanova, *Phys. Rev. B: Condens. Matter*, 2015, **91**, 024402.
28 M. Obstbaum, M. Härtinger, H. G. Bauer, T. Meier, F. Swientek, C. H. Back and G. Woltersdorf, *Phys. Rev. B: Condens. Matter*, 2014, 89.
29 Y. Ohnuma, H. Adachi, E. Saitoh and S. Maekawa, *Phys. Rev. B: Condens. Matter*, 2014, **89**, 174417.
30 K. Uchida, Z. Y. Qiu, T. Kikkawa, R. Iguchi and E. Saitoh, *Appl. Phys. Lett.*, 2015, **106**, 052405.
31 S. R. Boona and J. P. Heremans, *Phys. Rev. B: Condens. Matter*, 2014, **90**, 064421.
32 S. R. Etesami, L. Chotorlishvili, A. Sukhov and J. Berakdar, *Phys. Rev. B: Condens. Matter*, 2014, **90**, 014410.
33 A. E. White, *Experimental study of electron temperature fluctuations in the DIII-D tokamak*, ProQuest, 2008.
34 A. E. Clark and R. E. Strakna, *J. Appl. Phys.*, 1961, **32**, 1172–1173.
35 *Handbook of Optical Constants of Solids*, ed. E. D. Palik, Academic Press, Burlington, 1997, pp. xv–xvi, DOI: 10.1016/B978-012544415-6.50000-5.
36 G. B. Scott, D. E. Lacklison and J. L. Page, *Phys. Rev. B: Solid State*, 1974, **10**, 971–986.
37 P. Potera, S. Ubizskii, D. Sugak and K. Schwartz, *Acta Phys. Pol., A*, 2010, **117**, 181–183.
38 S. Bhagat, H. Lessoff, C. Vittoria and C. Guenzer, *Phys. Status Solidi A*, 1973, **20**, 731–738.
39 C. M. Srivastava and R. Aiyar, *J. Phys. C: Solid State Phys.*, 1987, **20**, 1119–1128.
40 A. Azevedo, L. H. Vilela-Leao, R. L. Rodriguez-Suarez, A. F. L. Santos and S. M. Rezende, *Phys. Rev. B: Condens. Matter*, 2011, **83**, 144402.